PCCP

Accepted Manuscript

ROYAL SOCIETY OF CHEMISTRY

www.rsc.org/pccp

PhysChemChemPhys

ARTICLE

Quantifying highly efficient incoherent energy transfer in perylene-based multichromophore arrays

Received 00th January 20xx,
Accepted 00th January 20xx

DOI: 10.1039/x0xx00000x

www.rsc.org/

James E. A. Webb,[a] Kai Chen,[b] Shyamal K. K. Prasad,[b] Jonathan P. Wojciechowski,[a] Alexander Falber,[a,c] Pall Thordarson,[a]* and Justin M. Hodgkiss[b]*

Multichromophore perylene arrays were designed and synthesized to have extremely efficient resonance energy transfer. Using broadband ultrafast photoluminescence and transient absorption spectroscopies, transfer timescales of approximately 1 picosecond were resolved, corresponding to efficiencies of up to 99.98%. The broadband measurements also revealed spectra corresponding to incoherent transfer between localized states. Polarization resolved spectroscopy was used to measure the dipolar angles between donor and acceptor chromophores, thereby enabling geometric factors to be fixed when assessing the validity of Förster theory in this regime. Förster theory was found to predict the correct magnitude of transfer rates, with measured ~2-fold deviations consistent with the breakdown of the point-dipole approximation at close approach. The materials presented, along with the novel methods for quantifying ultrahigh energy transfer efficiencies, will be valuable for applications demanding extremely efficient energy transfer, including fluorescent solar concentrators, optical gain, and photonic logic devices.

Introduction

Excitation energy transfer plays an important role in photonic systems ranging from photosynthesis, to excitonic solar cells, and as a molecular ruler for biophysical applications. Transfer efficiencies exceeding 90% are found in photosynthetic light harvesting systems,[1-4] where Förster Resonance Energy Transfer[5-8] (FRET) mechanisms have been demonstrated[9] and the role of quantum coherence is debated.[10]

Some applications of synthetic light harvesting materials are subject to non-linearities that demand extremely efficient energy transfer. For example, in dendritic light harvesting arrays,[11-16] efficiency losses along multistep pathways are cumulative, thus achieving 90% quantum efficiency in a 6-step cascade requires each step to exceed 98% efficiency. Likewise, in photonic information applications exploiting energy transfer,[17-21] loss of stepwise efficiency severely compromises the integrity of multistep logic operations. In optical gain media[22] and fluorescent solar concentrators[23] there is a stringent demand for emission from the final dilute acceptor to be as strong as possible and shifted away from the donor. If the acceptor emission is not shifted sufficiently far, or if poor energy transfer efficiency requires increasing the acceptor concentration, reabsorption from the donor or acceptor chromophores introduce losses that scale exponentially. Numerous examples exist of light harvesting arrays that undergo energy transfer on the picosecond timescale[24-31] however efficiencies beyond 90% are typically considered close enough to unity and not pursued further.

Synthetic systems remain guided by FRET theory of incoherent energy transfer, where the rate of energy transfer (k_{FRET}) from an excited donor to an acceptor is expressed in terms of their dipolar interaction at a given distance, R, relative to their Förster radius (R_0);

$$k_{FRET} = \frac{1}{\tau_D}\left(\frac{R_0}{R}\right)^6 \qquad (1)$$

where τ_D is the intrinsic lifetime of the donor and R_0 – the distance corresponding to a 50% probability of transfer - can be written as;

$$R_o^6 = \frac{9(\ln 10)k^2 Q_D}{128\pi^5 N_A n^4} J(\lambda) \qquad (2)$$

[a] School of Chemistry, the Australian Centre for Nanomedicine and the ARC Centre of Excellence in Convergent Bio-Nano Science and Technology, The University of New South Wales, NSW 2052, Australia. Email: p.thordarson@unsw.edu.au
[b] MacDiarmid Institute for Advanced Materials and Nanotechnology, and School of Chemical and Physical Sciences, Victoria University of Wellington, Wellington 6140, New Zealand. Email: Justin.Hodgkiss@vuw.ac.nz
[c] Flurosol Industries Pty. Ltd., Level 5, 574 St. Kilda Road, Melbourne, VIC 3004, Australia

† Footnotes relating to the title and/or authors should appear here.
Electronic Supplementary Information (ESI) available: Experimental procedures including synthesis of **1-3**, calculated structures, spectroscopic data acquisition and analysis methods. See DOI: 10.1039/x0xx00000x

Using this relationship, potential donor and acceptor pairs are evaluated in terms of the spectral overlap integral of the donor emission and acceptor absorption (J(λ)), their orientation factor (κ^2), and donor quantum yield (Q_D), where other terms are Avogadro's number (N_A) and refractive index of the medium (n).

The donor-acceptor separation, R, must be substantially less than R_0 in the regime of highly efficient transfer, however, the close proximity of donor and acceptor chromophores can invalidate key assumptions in the formulation of FRET theory.[32] First, FRET theory assumes weak coupling between independent donor and acceptor chromophores, rather than delocalized states that can form across closely positioned chromophores. Second, the point dipole approximation of FRET theory is only valid when the chromophore separation is much larger than the size of chromophores, otherwise different parts of chromophores will make stronger contributions to the Coulomb interaction than others. Classical extensions of FRET theory include extended dipole and line dipole models,[33-35] and atomistic transition density models.[36-37] New methods are required for quantifying extremely high transfer efficiencies in the regime of >99.9% in order to assess the performance of energy transfer materials as well as the applicability of FRET theory and extensions thereof. Steady state photoluminescence (PL) spectroscopy cannot resolve the small variations in donor or acceptor fluorescence intensities for systems in this highly efficient regime. Time-resolved PL spectroscopy enables efficiencies to be ascertained via measured transfer rates, however, it is essential to combine ultrafast (sub-picosecond) time resolution with broadband spectral resolution in order to distinguish between PL from the donor and acceptor and to verify that spectral signatures correspond to the weak-coupling regime.

Herein, we present a series of perylene-based arrays with strong resonant overlap between chromophores positioned

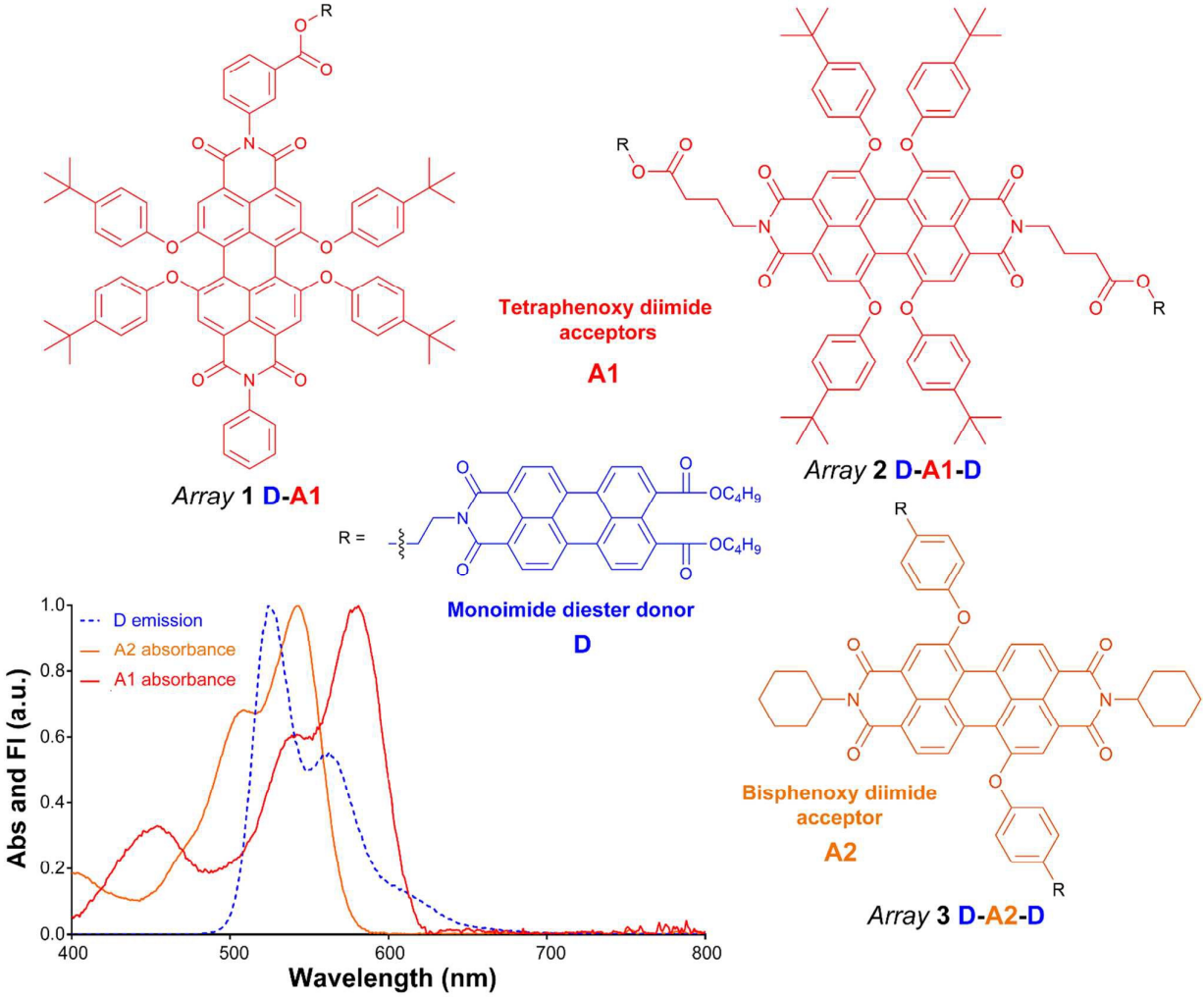

PhysChemChemPhys

ARTICLE

Fig. 1 Fluorescence spectra of the donor and absorption spectra of the acceptors used in this study, along with their molecular structures.

close together. We use a novel broadband ultrafast PL spectroscopy method, complemented by transient absorption (TA) spectroscopy, to resolve incoherent population transfer from the excited donor to the acceptor on a timescale of approximately 1 ps (confirming >99.9% efficiencies). Measurement of orientation factors via ultrafast depolarization permits explicit comparison with rate predictions via Förster theory, which points to deviations due to the breakdown of the point dipole approximation.

Results and discussion

Materials

Perylenes are hugely versatile fluorophoric components,[12,38] with good chemical, photo and structural stability, many possible configurations for coupling to other units, strong optical absorption, and emission quantum yields approaching unity. These properties and the photophysical parameters listed in Table 1 make them ideal for developing new materials for highly efficient light harvesting arrays. We have developed three light harvesting FRET arrays based upon the spectral overlap of two donor-acceptor pairs, selected for their strong resonance; monoimide diester as a donor (**D**, blue) paired with either a tetraphenoxy diimide (**A1**, red), or a bisphenoxy diimide (**A2**, orange) (Figure 1).

The monoimide diester is an exceptionally good donor as its asymmetric structure is easily synthetically accessible and permits well-defined placement in arrays. Also the donor emission strongly overlaps with the absorption of both tetraphenoxy diimide and bisphenoxy diimide, producing R_0 values exceeding 5 nm (Figure 1 and Table 1).

Table 1 Spectral overlap properties of the donor and acceptor components of multichromophore arrays **1**-**3**.

Array	Abs / Emission max (nm)		J (x 10^{15} nm^4/M cm)	R_0 (Å)[a]
	Donor	Acceptor		
Array **1**	507 / 524	585 / 618	2.36	54.8
Array **2**	506 / 524	540 / 611	2.53	55.4
Array **3**	509 / 524	545 / 572	2.80	56.3

[a]Calculated for $\kappa^2 = 2/3$, n =1.445 and $Q_D = 0.85$

The perylene arrays were synthesised with two linking strategies in mind; firstly conjugation via the imide position of the donor to the acceptor in arrays **1** and **2**, and secondly from the imide of the donor to the 'bay' position of the acceptor in array **3**. The donor synthesis in both of these strategies was similar; using established chemistry asymmetry about the peri-positions was induced, forming a monoanhydride Perylene dibutyl ester.[39] The precursor donor perylene is then reacted with the respective amine in dimethylformamide at 110 °C, which rapidly condenses to the donor perylene monoimide di-

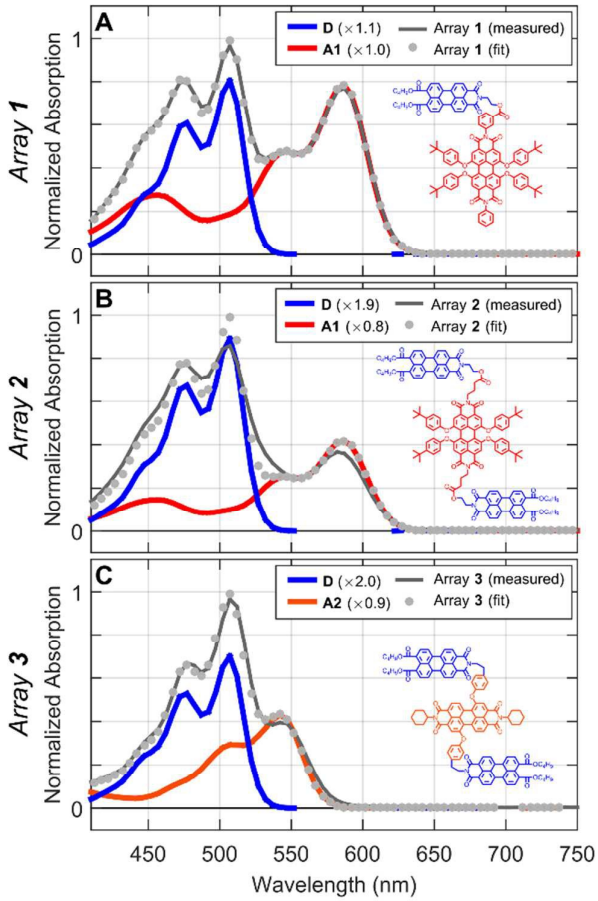

Fig. 2 Structures and UV-vis absorption spectra of (A) array **1**, (B) array **2**, and (C) array **3**, each fitted to a sum of the constituent reference monomers also shown (**D**, **A1**, and **A2**).

esters in over 80% yield. The core perylenes for arrays **2** and **3** were obtained from condensation of the dianhydride with the desired amine in high yields, while the core of **1** was obtained from a statistical mixture of two different amines in approximately 30% yield. Arrays **1** and **3** were obtained in 3% and 40% yield by reaction of the acid chloride of the respective core and the ethanolimide donor. Array **2** was obtained by the reaction of the phenolic tyrimide derivative with the 1,7-dibromo core in the presence of potassium carbonate in 75% yield.

As a starting point, low-level universal force field (UFF) calculations were performed to obtain the dimensions of donor, acceptor and linker units, along with the minimized structure in the case of the more rigid array **3**. A number of Theoretical predictions of FRET rates will be discussed later, but it is worth noting that given predicted R_0/R values on the order of 3 would correspond to FRET timescales on the order of 1 ps and high efficiencies of over 99.9%.

Spectroscopy

Steady-state absorption spectroscopy. An important condition for the validity of Förster theory is the independence of each individual chromophore. When this condition is compromised through excitonic or excimeric coupling of the donor and/or acceptor species, their absorption and emission spectra are expected to differ significantly from the parent constituents and Förster theory cannot be simply applied.[32] To verify the weak coupling regime where Förster theory remains valid, it is possible to compare the absorption spectra with the linear sum

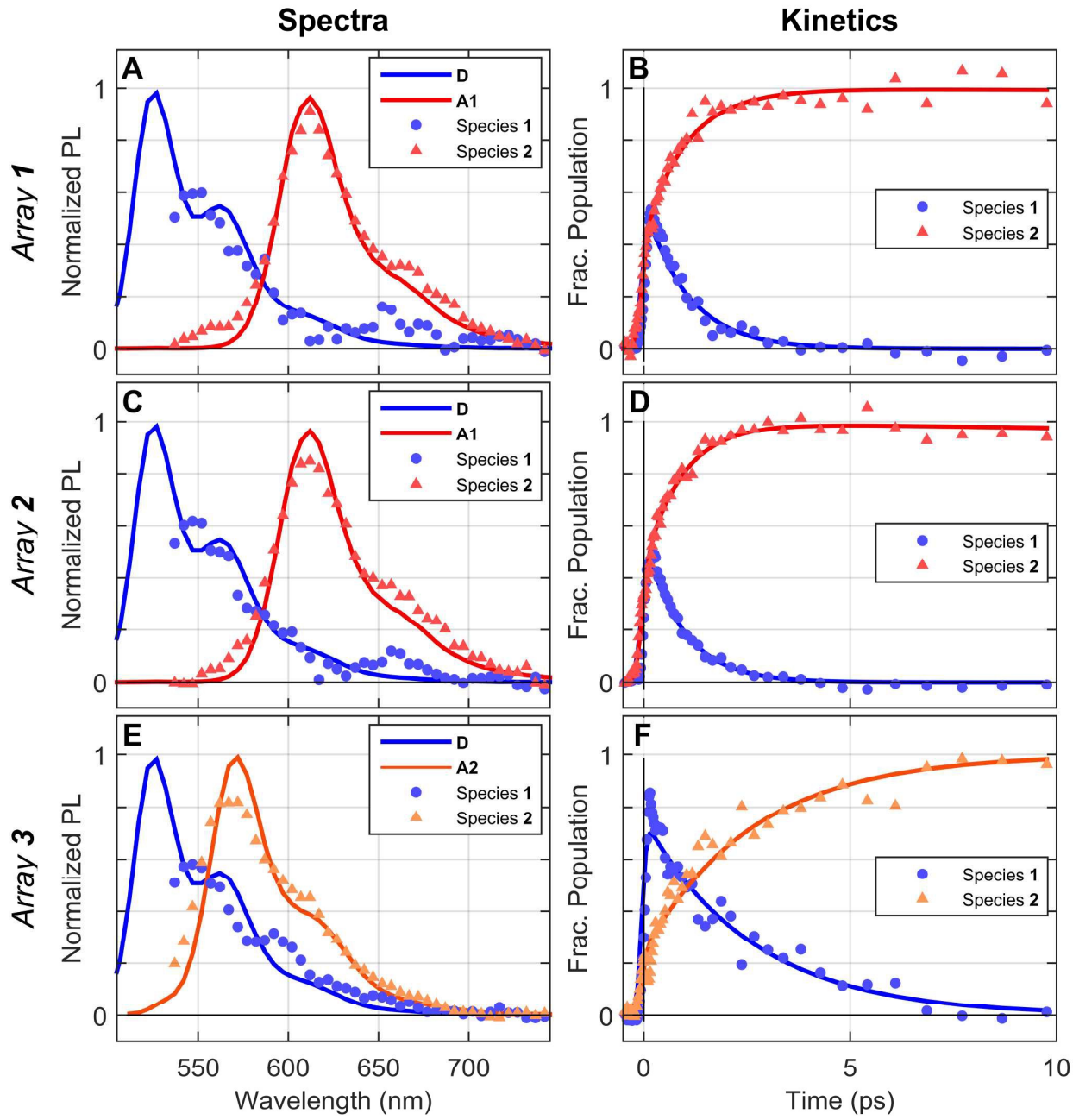

Fig. 3 Ultrafast PL spectra of the multichromophore arrays used in this study. The three compounds comprise rows; array **1** (first row, panels (A)-(B)), array **2** (2nd row, panels (C)-(D)), and array **3** (3rd row, panels (E)-(F)). Ultrafast PL spectra (left column) and kinetics (right column) components extracted from bilinear decompositions of the surfaces, labelled species 1 and 2. Spectra of the reference monomers **D**, **A1**, and **A3** are also shown. The full PL surfaces are provided in the ESI

of the constituent spectra. The analysis of absorption spectra shown in Figure 2 confirms that the array spectra are well described by a linear sum of constituent components, suggesting the absence of perturbative intramolecular or intermolecular effects. This conclusion is also supported by the analysis of transient spectra below (Figures 3 and 4).

Ultrafast PL spectroscopy. Since FRET transfer efficiencies are predicted to exceed 99.9% in these arrays, steady state fluorescence spectroscopy is an insensitive measure of transfer rates and efficiencies. Instead, transfer rates were directly resolved using a broadband ultrafast PL method that we recently developed – transient gating PL spectroscopy.[40] By using a transient grating effect to gate broadband spectra, excited donor and acceptor signatures can be cleanly resolved from ultrafast timescales, including in the spectral region where long-lived emission from the acceptor emission would produce a prohibitively large background using the previously used broadband ultrafast PL method of optical Kerr gating.[41]

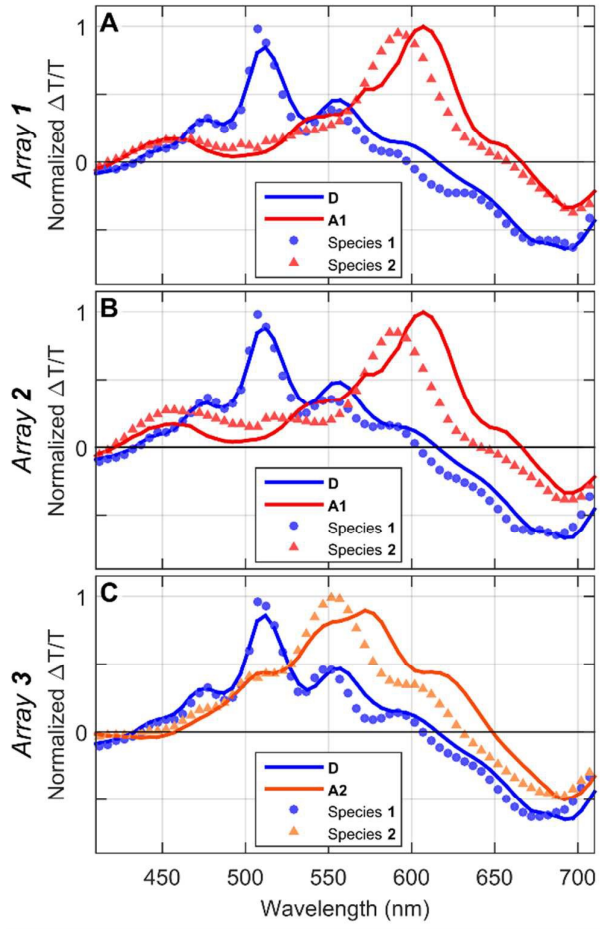

Fig. 4 Ultrafast TA spectra extracted from a bilinear decomposition of the TA surfaces for arrays **1**-**3** (full data in ESI) compared with the relevant reference monomer spectra. In each case, species 1 converts to species 2 on the timescale given in Table 2.

Figure 3 shows spectra and associated kinetic components extracted from a bilinear decomposition of the ultrafast PL surfaces (full surfaces and residuals from this bilinear fit are provided in the ESI).

In these measurements, the samples were excited with 100 fs pulses at 500 nm, which according to the decomposed UV-vis absorption spectra in Figure 2 corresponds to 80, 89, and 69% absorption by the donor component for compounds **1**, **2**, and **3**, respectively. The ultrafast spectral components identified in arrays **1** and **2** (labelled as species 1 and 2) clearly match the steady state spectra of the isolated donor and acceptor components that are also shown in the figure, including their vibronic structure. This correspondence again confirms the weak-coupling regime – PL is associated with localized excitations on either the donor or acceptor components. The blue edge of the ultrafast spectra (including the donor emission peak) is obscured by the filter used to remove scattered excitation light. The filter, along with the smaller spectral separation between donor and acceptor components makes it difficult to deconvolute the spectral components of array **3**. Nevertheless, transfer kinetics were clearly resolved from the bilinear decompositions of each of the arrays, corresponding to population decay of the excited donor and growth of the excited acceptor signatures. The measured kinetics were fit to global monoexponential decay functions with time constants of 1 ps (array **1**), 0.9 ps (array **2**), and 2.5 ps (array **3**).

Ultrafast TA spectroscopy. The FRET dynamics were confirmed using ultrafast TA spectroscopy. Using the same bilinear decomposition approach, TA spectra and associated kinetics components are presented in Figure 4. Again, the TA spectra attributed to donor and acceptor components of the FRET arrays (labelled species 1 and 2) match those obtained for isolated respective monomers, although the acceptor spectra appear to be slightly blue-shifted with respect to the reference monomers. Each component features a strong ground-state bleach ($\Delta T/T>0$), with stimulated emission ($\Delta T/T>0$) and photoinduced absorption ($\Delta T/T<0$) features appearing progressively to the red. This manifold of features is redder for the acceptors than the donors. Moreover, the measured lifetimes (0.7 ps, 0.5 ps, and 1.5 ps) are in reasonable agreement with those measured *via* ultrafast PL spectroscopy. Although the TA surfaces on their own may be difficult to definitively interpret, owing to overlapping positive and negative signals from the different species, the combination of ultrafast broadband PL and TA measurements provides robust measurements of FRET rates.

FRET efficiencies. To ascertain the efficiency of energy transfer, the lifetime of the monomeric donor reference compound is compared to the lifetime of the donor in within the array. The reference donor lifetime was measured using time correlated single photon counting (TCSPC), and was found to be 4.47 ns (see ESI). FRET efficiencies were then calculated using Equation 3:

$$\phi = 1 - \left(\frac{\tau(array\ donor)}{\tau(free\ donor)}\right) \quad (3)$$

Using this relationship arrays **1**-**3** all exhibit energy transfer efficiencies of over 99.9% (Table 2), as expected from the high ratio of R_0:R ratio Table 1. In the case of the array **2**, for example, the transfer efficiency of 99.98% is sufficient that a photonic process depending on 50 transfer steps would still be 99% efficient. Supposing that a single transfer efficiency was measured via a method (e.g., steady state PL spectroscopy) that could only resolve the step-wise efficiency as 95±5%, the cumulative error would lead to meaningless predicted 50-step transfer efficiencies ranging from only 0.5% to 100%. The TCSPC measurements also provided further support for the weak-coupling regime by confirming that the acceptor lifetimes in the arrays closely matched (within 10%) the lifetimes of the respective acceptor monomers (see ESI).

Comparison with theoretical rate predictions. Before assessing the validity of Förster theory in the ultrafast transfer regime, it is essential to constrain the geometric parameters κ^2 and R using experimental measurements. While the dynamically averaged value of κ^2 = 2/3 is routinely assumed, it is inadequate to describe energy transfer on the ultrafast timescale that dipolar geometry is essentially static. The choice of a value of κ^2 between 0 and 4 has a large effect on the predicted transfer rate, as does the R value owing to its R^6 scaling, and both should therefore be fixed from structural data or otherwise constrained from measurements. Solution or solid-state structures are not available for arrays **1**-**3**, and in the case of **1** and **2**, conformational flexibility is likely. However, ultrafast PL depolarization can be used to measure the effective dipolar angle between the donor and acceptor. Using these measurements to inform simple molecular models leads to viable combinations of κ^2 and R and ultimately predicted FRET rates via Equations 1 and 2.

κ^2 is expressed in terms of the three angles (Figure 5a) needed to define two arbitrary dipoles interacting through space according to equation 4:

$$\kappa^2 = (cos\theta_T - 3cos\theta_D cos\theta_A)^2 \quad (4)$$

In the case of arrays **1**-**3**, the direct tethering of donor and acceptor molecules means that their transition dipole vectors (long axis of the molecule) can be approximated as intersecting at an angle θ_T, as depicted in Figure 5b. θ_T is related to the polarization anisotropy, r, which is measured as;

$$r = (I_{\parallel} - I_{\perp})/(I_{\parallel} + 2I_{\perp}) \quad (5)$$

where $I_{\parallel}$ and $I_{\perp}$ are the measured PL intensities polarized parallel and perpendicular to the excitation polarization, respectively. On the ultrafast timescale before fluorophores can physically rotate, an isolated fluorophore is expected to yield the maximum value of r = 0.4, corresponding to aligned absorption and emission transition dipoles. When the emitting dipole is rotated with respect to the absorption dipole, for example when emission occurs from an acceptor following FRET from the donor, polarization anisotropy is expressed in terms of the angular displacement (θ_T) between absorption and emission dipoles;[42]

$$r = 0.4\left(^3/_2\, cos^2\theta_T - {}^1/_2\right) \quad (6)$$

The measured θ_T angles could arise from either of the two general conformations depicted in Figure 5b - the measured polarization anisotropy reflects the projected intensities (~$cos^2\theta_T$), which are equivalent in each case. The implications of the dual solutions will be discussed for each molecule.

The transient grating PL spectroscopy method was used to measure the polarization anisotropy of acceptor PL following excitation of the donor and polarization resolved ultrafast PL detection. It was essential to separate contributions of the donor and acceptor to the overall PL anisotropy, which would not have been straightforward using conventional single channel PL detection methods. However, with broadband PL detection, we applied the global fitting approach described above to extract pairs of PL spectra and kinetics from PL

Table 2 Predicted and measured FRET parameters for multichromophore arrays **1**-**3**.

Array	Measured θ_T[a]	R (Å)[b]	κ^2[b]	Calculated FRET lifetime (ps)[c]	Measured FRET lifetime (ps)		Measured FRET efficiency (%)[d]	
					PL	TA	PL	TA
Array **1**	θ_{T1}: 56°	9.6	3.2	0.19	1.0	0.6	99.98	99.98
	θ_{T2}: 124°	18	0.5	1.2				
Array **2**	θ_{T1}: 58°	9.5	3.1	0.13	0.9	0.6	99.98	99.99
	θ_{T2}: 122°	17	0.6	0.91				
Array **3**	θ_T: 69°	17.2	0.5	4.8	2.6	1.0	99.94	99.97

[a]From ultrafast depolarization measurements described in the text and illustrated in Figure 5B. [b]Calculated from structures using the measured θ_T values, and the lengths of the chromophores and linking unit. [c]Calculated by applying Equations 1 and 2 to the relevant parameters listed in Table 1 and here. [d]Calculated by applying equation 3 to the measured FRET lifetimes, taking the unquenched τ_D = 4.5 ns.

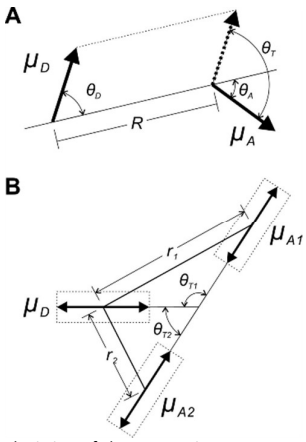

Fig. 5 (A) Schematic depiction of the geometric parameters defining the orientation factor κ^2 in Equation 4. (B) Depiction of the simplified geometry corresponding to dipoles directly tethered to each other, leading to the measurement of θ_T from r in Equation 6.

surfaces measured parallel and perpendicular to the excitation polarization. Since the surfaces were well described by this bilinear decomposition (residuals shown in ESI), r could be calculated from the time-dependent spectral amplitudes. Since it was not possible to selectively excite the donor due to spectral overlap, the anisotropy contribution from the directly excited acceptor must also be removed. Assuming that the directly excited acceptor has anisotropy of r = 0.4, its weighted contribution was subtracted from the measured data based on the known excitation ratio's in the UV-vis spectral decomposition in Figure 2.

Measured and corrected time-dependent anisotropy values for compounds **1-3** are shown in Figure 6. First, we can check the validity of the method by verifying that the anisotropy values extracted for the donor components begin near the maximum value of 0.4. Since anisotropy (Equation 5) is normalized by the total PL intensity, transfer from the donor to the acceptor results in a diminishing denominator and thus an increase in noise over time. Having confirmed that the global analysis method cleanly separates the contributions of donor and acceptor, we examined the PL anisotropy for the acceptor components. The most reliable estimate of anisotropy comes from the corrected values at a time when transfer is complete, yet too early for physical tumbling of the fluorophores to cause further depolarization. Averaging the acceptor anisotropies (corrected for the contribution of direct acceptor excitation) from 5-10 ps results in r-values of between -0.01 and -0.13 (Figure 6 and Table 2). In systems with conformational disorder, these can be considered the expectation values of polarization anisotropy.Applying Equation 6 to the measured r-values results in pairs of θ_T angles (according to the two general conformations in Figure 5b) of 56°/124° (array **1**), 58°/122° (array **2**) and 69°/111° (array **3)**. While trimer arrays **2** and **3** feature two donor chromophores, their symmetric equivalence allows us to consider the possible donor/acceptor dipolar conformations as if they were dimers. The flexible nature of the linker units in array **1** and array **2** mean that both conformations are viable from a molecular perspective. While the more open conformation has a higher κ^2 value than the folded conformation, the greater chromophore separation will offset the boost in predicted rate. The combined effects of κ^2 and R on the predicted rates were calculated by applying equations 1 and 2 to calculate FRET rates when modelling the donor and acceptor chromophores as 0.88 and 1.16 nm long and linked by a hinge of radius d = 0.47 nm (array **1**) or 0.43 nm (array **2**) (based on UFF models in the ESI). These calculations showed that the folded conformations resulted in predicted FRET rates of 5.3 × 10^{12} s^{-1} (τ = 0.19 ps) for **1** and 7.8 × 10^{12} s^{-1} (τ = 0.13 ps) for **2** (Table 2), while the more extended conformations led to theoretical FRET rates of 8.4 ×10^{11} s^{-1} (τ = 1.2 ps) and 1.1 ×

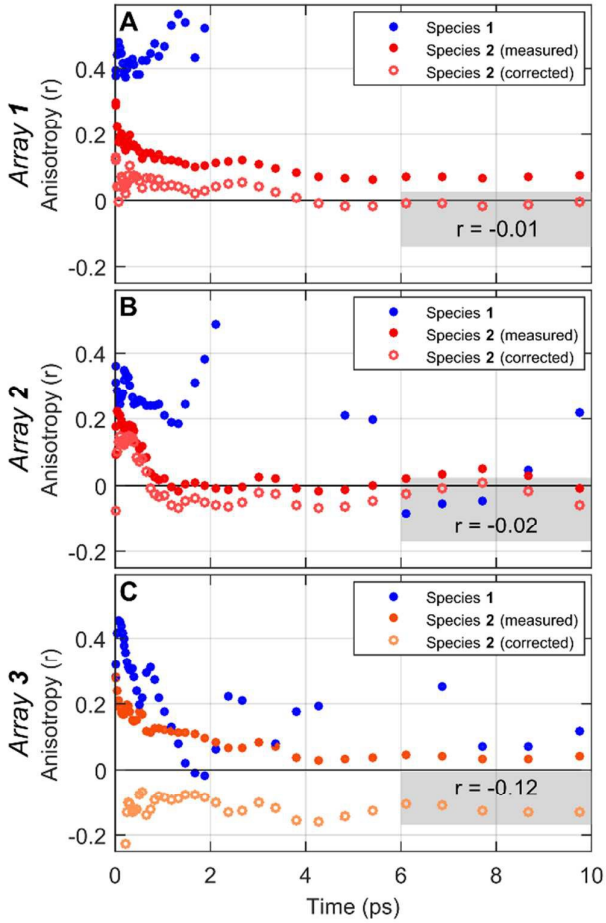

Fig. 6 (A)-(C) Measured polarization anisotropy for arrays **1-3**, where the donor and acceptor spectroscopic species were separated via a bilinear decomposition The corrected acceptor anisotropy accounts for the small fraction of directly excited

acceptor chromophore. The final corrected anisotropy values are noted in the text boxes.

10^{12} s^{-1} (τ = 0.91 ps), respectively.

In the case of array **3**, the donor and acceptor chromophores are connected in a comparatively rigid conformation. After verifying that the θ_T predicted by a molecular mechanics model (63°, ESI) was reasonably close to the polarization anisotropy measurement of 69°, κ^2 and R-values were taken directly from the modelled structure to arrive at the predicted FRET rate of 2.1 × 10^{11} s^{-1} (τ = 4.8 ps) using Equations 1 and 2 (Table 2).

Starting with array **3**, where the rigid structure gives unambiguous R and κ^2 values, it is clear that the FRET rate measured via ultrafast PL spectroscopy is ~2-fold higher than the FRET prediction. This discrepancy likely reflects the breakdown of the point dipole model.[36-37] The higher observed rates reflect the dominance of transition density at separations shorter than the centre-to-centre distance in the point dipole approximation. Langhals *et al* also observed appreciable FRET rates in a rigid donor-acceptor pair, which was surprising given the rigid orthogonal geometry for which κ^2 and theoretical Förster rate = 0.[27] In that case, the observed deviation was attributed to symmetry breaking vibrational modes.

For arrays **1** and **2**, the conformational ambiguity described above produces pairs of theoretical predictions to compare with experimental observations. The rates via ultrafast PL spectroscopy are ~5-7-fold slower than FRET predictions for the folded conformations (θ_T~60°), and slightly faster than predictions for the open conformations (θ_T~120°). Interestingly, atomistic corrections to Förster theory would also predict suppressed rates for folded conformations and enhanced rates for open conformations. Wiesenhofer *et al* calculated the deviation from Förster theory for model donor-acceptor systems topologically similar to ours, featuring donor and acceptor molecules tethered by a virtual hinge.[36] They found that Förster theory overestimated transfer rates by a factor of ~2 when the donor and acceptor were displaced at an angle of 60°, and underestimated transfer rates by a factor of ~2 for 120° displacement. Although we cannot determine which conformation dominates in our experimental model systems, breakdown of the point dipole approximation at close approach is the likely explanation of the observed deviation from Förster theory predictions for either conformation. We note that quantitatively accounting for deviation from Förster theory in our system requires considering the explicit molecular orbitals and structures (i.e., they cannot be taken from simulations of a different model system). The observed deviations from Förster theory may be assessed in greater detail in the future by applying our methods to rigid multichromophore arrays for which structures are precisely known. By examining the deviation as a function of the angles and distance defining the dipolar interaction of the two chromophores, measurements of the type we described here may be directly compared with atomistic transition density calculations where dipolar interactions are distributed according to the participating molecular orbitals. While measurements for rigid arrays may experimentally establish the size of corrections required, such corrections do not appear to change the magnitude of rates predicted by Förster theory, even for closely separated chromophores with ultra-high transfer efficiencies. Moreover, such corrections are still made within the semiclassical framework of incoherent energy transfer, which is appropriate given the spectral signatures we observed for transfer between localized states.

Conclusions

In conclusion, we have synthesized a series of perylene-based multichromophore arrays with highly efficient energy transfer. We applied a new broadband ultrafast PL spectroscopy method to resolve transfer timescales of approximately 1 ps, and spectral signatures consistent with incoherent energy transfer between localized states. Polarization resolved measurements also allowed us to constrain geometric parameters (the dipolar angle between donor and acceptor units) and thereby compare our measurements to theoretical rate predictions using Förster theory. We found that Förster theory predicted transfer rates of the correct magnitude, but deviations of ~2-fold (and possibly higher, subject to conformational uncertainty) were attributed to the breakdown of the point dipole approximation at close approach. With transfer efficiencies of up to 99.98%, the materials presented may be effective components of fluorescent solar concentrator films. Moreover, the broadband ultrafast PL methods developed here can be applied in the future to other light harvesting arrays and photonic systems where non-linearities mean that ultrahigh stepwise transfer efficiencies essential.

Acknowledgements

This research is supported by Flurosol Industries Pty Ltd[‡] and an Australian Research Council (ARC) Linkage Project Grant to PT, AF and JMH (LP130100774) and an ARC Centre of Excellence Grant (CE140100036) and ARC Future Fellowship to PT (FT120100101). JMH also acknowledges support from a Rutherford Discovery Fellowship.

Notes and references

[‡]AF has equity in Flurosol Industries Pty. Ltd who did support this work.

1 X. Hu, A. Damjanovic, T. Ritz and K. Schulten, *Proc. Nat. Acad. Sci. U.S.A.*, 1998, **95**, 5935-5941.

2 V. Sunsdtrom, T. Pullerits and R. van Grondelle, *J. Phys. Chem. B*, 1999, **103**, 2327-2346.

3 G. R. Flemming and R. van Grondelle, *Acc. Chem. Res.*, 1996, **29**, 381-389.
4 G. R. Flemming and R. van Gondelle, *Curr. Opin. Struct. Biol.*, 1997, **7**, 738-748.
5 T. Förster, *Z. Naturforsch. A:Phys. Sci.*, 1949, **4a**, 321-327.
6 T. Förster, *Discus. Faraday Soc.*, 1959, **27**, 7-17.
7 V. I. Keteskemséty, *Z. Naturfosch. A:Phys. Sci.*, 1962, **17a**, 666-670.
8 S. A. Latt, H. T. Cheung and E. R. Blout, *J. Am. Chem. Soc.*, 1965, **87**, 995-1003.
9 M. Sener, J. Strumpfer, J. Hsin, D. Chandler, S. Scheuring, C. N. Hunter and K. Schulten, *ChemPhysChem*, 2011, **12**, 518-531.
10 G. S. Engel, T. R. Calhoun, E. L. Read, T. K. Ahn, T. Mancal, Y. C. Chen, R. E. Blankenship and G. R. Fleming, *Nature*, 2007, **446**, 782-786.
11 A. Adronov and J. M. J. Fréchet, *Chem. Comm.*, 2000, 1701-1710.
12 M. R. Wasielewski, *Acc. Chem. Res.*, 2009, **42**, 1910-1921.
13 P. D. Frischmann, K. Mahata and F. Würthner, *Chem. Soc. Rev.*, 2013, **42**, 1847-1870.
14 S. Sengupta and F. Würthner, *Acc. Chem. Res.*, 2013, **46**, 2498-2512.
15 L. Flamigni, B. Ventura, C.-C. You, C. Hippius and F. Würthner, *J. Phys. Chem. C*, 2007, **111**, 622-630.
16 R. F. Kelley, W. S. Shin, B. Rybtchinski, L. E. Sinks and M. R. Wasielewski, *J. Am. Chem. Soc.*, 2007, **129**, 3173-3181.
17 P. Bairi, P. Chakraborty, B. Roy and A. K. Nandi, *Sensors Actuat. B-Chem.*, 2014, **193**, 349-355.
18 A. P. de Silva and S. Uchiyama, *Nat. Nanotechnol.*, 2007, **2**, 399-410.
19 J. Li, Y.-Q. Huang, W.-S. Qin, X.-F. Liu and W. Huang, *Polym. Chem.*, 2011, **2**, 1341-1346.
20 T. Nishimura, Y. Ogura and J. Tanida, *Appl. Phys. Lett.*, 2012, **101**, 233703.
21 T. Nishimura, R. Fujii, Y. Ogura and J. Tanida, *Appl. Phys. Lett.*, 2015, **107**, 013701.
22 S. Chénais and S. Forget, *Polym. Int.*, 2012, **61**, 390-406.
23 J. S. Batchelder, A. H. Zewail and T. Cole, *Appl. Opt.*, 1979, **8**, 3090-3110.
24 C. Hippius, I. H. M. van Stokkum, M. Gsanger, M. M. Groeneveld, R. M. Williams and F. Würthner, *J. Phys. Chem. C*, 2008, **112**, 2476-2486.
25 M. J. Ahrens, R. F. Kelley, Z. E. Dance and M. R. Wasielewski, *Phys. Chem. Chem. Phys.*, 2007, **9**, 1469-1478.
26 M. Cotlet, T. Vosch, S. Habuchi, T. Weil, K. Müllen, J. Hofkens and F. de Schryver, *J. Am. Chem. Soc.*, 2005, **118**, 16941-16950.
27 H. Langhals, A. J. Esterbauer, A. Walter, E. Reidle and I. Pugliesi, *J. Am. Chem. Soc.*, 2010, **132**, 16777-16782.
28 C. Ramanan, C. H. Kim, T. J. Marks and M. R. Wasielewski, *J. Phys. Chem. C*, 2014, **118**, 16941-16950.
29 S. M. Dyar, J. C. Barnes, M. Juricek, J. F. Stoddart, D. T. Co, R. M. Young and M. R. Wasielewski, *Angew. Chem. Int. Ed.*, 2014, **53**, 5371-5375.
30 K. E. Brown, W. A. Salamant, L. E. Shoer, R. M. Young and M. R. Wasielewski, *J. Phys. Chem. Lett.*, 2014, **16**, 23735-23742.
31 E. A. Margulies, L E. Shoer, S. W. Eaton and M. R. Wasielewski, *Phys. Chem. Chem. Phys.*, 2014, **16**, 23735-23742.
32 D. Beljonne, C. Curutchet, G. D. Scholes and R. J. Silbey, *J. Phys. Chem. B*, 2009, **113**, 6583-6599.
33 W. J. Beenken and T. Pullerits, *J. Chem. Phys.*, 2004, **120**, 2490-2495.
34 S. Westenhoff, C. Daniel, R. H. Friend, C. Silva, V. Sundstrom and A. Yartsev, *J. Chem. Phys.*, 2005, **122**, 094903.
35 T. Renger, *Photosynth. Res.*, 2009, **102**, 471-485.
36 H. Wiesenhofer, D. Beljonne, G. D. Scholes, E. Hennebicq, J. L. Brédas and E. Zojer, *Adv. Funct. Mat.*, 2005, **15**, 155-160.
37 Y. R. Khan, T. E. Dykstra and G. D. Scholes, *Chem. Phys. Lett.*, 2008, **461**, 305-309.
38 F. Würthner, C. R. Saha-Moller, B. Fimmel, S. Ogi, P. Leowanawat and D. Schmidt, *Chem. Rev.*, 2015, DOI:10.1021/acs.chemrev.5b00188.
39 C. Xue, R. Sun, R. Annab, D. Abadi and S. Jin, *Tet. Lett.*, 2009, **50**, 853-856.
40 K. Chen, J. K. Gallaher, A. J. Barker and J. M. Hodgkiss, *J. Phys. Chem. Lett.*, 2014, **5**, 1732-1737.
41 K. Chen, A. J. Barker, M. E. Reish, K. C. Gordon and J. M. Hodkiss, *J. Am. Chem. Soc.*, 2013, **135**, 18502-18512.
42 R. E. Dale, J. Eisinger and W. E. Blumberg, *Biophys. J.*, 1979, **26**, 161-193.